www.cadanda.com
Computer-Aided Design AND APPLICATIONS

Research on Profile Geometric Feature Parameters Extraction of Complicated Thin-Walled Ring Parts with Irregular Section

Haonan Pei[1,2], Ming Luo[1,3] and Sizhe Du[1,2]

[1]Key Laboratory of High-Performance Manufacturing for Aero Engine (Northwestern Polytechnical University), Ministry of Industry and Information Technology, Xi'an 710072, China
[2]Engineering Research Center of Advanced Manufacturing Technology for Aero Engine, Ministry of Education, Northwestern Polytechnical University, Xi'an 710072, China
[3]State Key Laboratory of Cemented Carbide, Zhuzhou Hunan 412000, China

Corresponding author: Ming Luo, luoming@nwpu.edu.cn

Abstract. The extraction of profile geometric feature parameters (PGFPs) of complicated thin-walled ring parts with irregular section (CTWRPIC) plays an important role in the entity reconstruction and the establishment of automatic process planning knowledge base. Take the metallic W-ring of aero-engine as an example, due to the large number of rolling forming passes and the large difference in section profile shape, it is difficult to complete the effective extraction of multi-pass PGFPs. Besides, during the rolling forming process, the uneven organization of the billet, roller wear, etc. is likely to cause different lengths of the sealing lips on both sides of the metallic W-ring, which will lead to inaccurate parameter extraction results. To overcome these problems, this article proposes an adaptive bounding box based multi-pass PGFPs extraction method. First, based on the Andrew algorithm, the section profile point cloud with large differences in the shape of each pass is converted into the corresponding convex hull with similar shape, so as to improve the efficiency and stability of building of bounding box. Second, the slope of the convex hull vertices is used to identify whether the metallic W-ring has forming defects, so as to build an adaptive bounding box that more closely approximate the section profile point cloud. The robustness and accuracy of the method is demonstrated by the inspection experiments of PGFPs on the metallic W-ring samples from six rolling forming passes, compared with traditional standard inspection method, the relative error of our method is around 1%.

Keywords: PGFPs, CTWRPIC, metallic W-ring, adaptive bounding box
DOI: https://doi.org/10.14733/cadaps.2023.1271-1287

1 INTRODUCTION

CTWRPIC is a class of parts widely used in aviation, aerospace, nuclear power and other fields, take the metallic W-ring of aero-engine as an example, its sealing performance is of great

significance to reduce the engine internal flow loss and improve the engine thrust-weight ratio [8]. The profile forming accuracy of the metallic W-ring will affect its sealing performance to a large extent, therefore, accurate and efficient measurement of the profile is very important for the design and manufacture of the metallic W-ring. The traditional inspection method of metallic ring is destructive sampling, i.e., cutting it in the radial orientation and obtaining the results by inspecting the cut-off surface, however, this method is time consuming, costly and results in incomplete inspection of the quality of the parts in actual use. With the development of measuring instruments, measurement methods based on coordinate measuring machine (CMM) equipped with scanning probe are increasingly researched and used for the reason that they improve the measurement efficiency and retain the high precision of contact measurement methods [20,25,33], however, profile measurement of metallic W-ring based on CMM is impractical because the structural characteristics of the part severely limit the accessibility of the probe. In recent years, optical measurement methods have attracted a lot of attention due to its non-contact, high efficiency and flexibility [18,31].

Metallic W-ring has the characteristics of multi-pass rolling forming, closed ring structure, complex section profile and small size, it is difficult to design computer aided design (CAD) model of each rolling forming pass in short cycle and low cost. The inverse modeling solution based on point cloud slicing is an effective way to reconstruct the CTWRPIC, however, the lack of feature representation usually results in inaccurate and inconsistent topological CAD model. Consequently, it is difficult to represent the original design intention and to modify the final model parameters in an effective way [17]. On the other hand, to increase the level of automation of the different tasks involved in the planning of activities of the production cycle is a concern required every day more and more [21], computer aided process planning (CAPP) serves as a bridge between CAD and computer aided manufacturing (CAM) [26], enabling the production of products with higher quality, shorter manufacturing lead times and lower costs. In multi-pass plastic forming processes, the parametric representation of intermediate part geometrical features is the basis for the automatic process planning knowledge base. For the extraction of geometric feature parameters of parts, Gadelmawla [13] designed a non-contact measurement system to measure and inspect most spur gear parameters with appropriate accuracy. Li et al. [19] proposed a single/multi section parameters calculation method for blade based on optical scanning. Peng et al. [23] used computer vision technology to measure and extract the inner diameter and thickness of O-ring. Cheng et al. [9] measured the cooling hole diameter of turbine blade based on the stereo vision 3D reconstruction technique. However, in the existing works, there is no relevant research on the extraction of geometric feature parameters of the metallic W-ring.

In this article, we attempt to design a method for extracting PGFPs from CTWRPIC, which will be an important component of reconstructing entity and building knowledge base for automatic process planning, however, for CTWRPIC, the extraction of PGFPs is a challenging task. First, the metallic W-ring is usually made of high-temperature alloy material, which needs to be rolled with multiple passes and small deformation under the action of multiple sets of rollers before they can be finally formed. In order to realize the accurate forming, the CAD model of each pass needs to be designed, and the deformation is accurately allocated to each pass. Therefore, the extraction of PGFPs should consider all passes, but the profile shape of each pass is quite different, and it is difficult to complete the effective extraction of multi-pass PGFPs. Secondly, during the rolling forming process, the uneven organization of the billet, roller wear, etc. is likely to cause different lengths of the sealing lips on both sides of the metallic W-ring, which will lead to inaccurate parameters extraction results. In order to solve the above problems, we propose an adaptive bounding box based multi-pass PGFPs extraction method, the slope of the convex hull vertices is used to identify whether the metallic W-ring under each rolling forming pass has forming defects, so as to build an adaptive bounding box that more closely approximate the section profile point cloud. Based on the adaptive bounding box based multi-pass PGFPs extraction method and a designed optical measurement system, a method to inspect PGFPs from CTWRPIC is proposed. The main contributions are as follows:

(1) Quickly calculate the convex hull of the section profile point cloud during the multi-pass rolling forming of metallic W-ring based on Andrew algorithm [1], which transforms the profile point cloud of each rolling forming pass with a large difference in shape into the corresponding convex hull of similar shape, so that the efficiency and stability of building the bounding box of each pass can be improved.

(2) An adaptive bounding box based multi-pass PGFPs extraction method is proposed, which determines whether there is a significant length difference between the sealing lips on both sides of the metallic W-ring based on the slope of the convex hull vertices, so as to build an adaptive bounding box that more closely approximate the section profile point cloud.

(3) Through the adaptive bounding box based multi-pass PGFPs extraction method and the designed measurement system, a method to inspect PGFPs from CTWRPIC is realized. Extensive experimental results demonstrate that our method shows better accuracy and robustness compared with the existing methods.

The rest of this article is organized as follows. In Section 2, the related works are reviewed. In Section 3, the designed measurement system is briefly described, the motivation behind our method is presented and our method is given. In Section 4, the adaptive bounding box based multi-pass PGFPs extraction method is introduced in detail. In Section 5, the method to inspect PGFPs from CTWRPIC and the experimental set up are given. In Section 6, the experimental results and the comparison of different methods are presented and discussed. Finally, Section 7 conclude this article.

2 RELATE WORK

In this section, the algorithms involved in the related work are reviewed.

2.1 Convex Hull

The fast computation of convex hull of point set (suppose it contains *n* points) has been one of the fundamental problems in computational geometry [15] and is widely used in pattern recognition, image processing and artificial intelligence. Well-known convex hull algorithms mainly include Graham scan algorithm [14], Jarvis march algorithm [16], Divide and Conquer algorithm [24], "Quickhull" algorithm [5,11] and Andrew algorithm.

Graham scan algorithm is often referred to as the first algorithm for computational geometry [21], its idea is to consistently look though the ordered list and use angle measurements to remove points that are not in the convex hull, Graham scan algorithm time complexity is $O(n\log n)$, however, the algorithm is much slower due to the use of triangular instructions, and less efficient when the point scale is large. Instead of focusing on the extreme points, Jarvis march algorithm introduces the idea of checking edges when entering a convex hull, which starts with one endpoint of an extreme edge to find another extreme edge, and so on until a loop is formed, the algorithm is not based on ordering and its time complexity at the end of the convex hull calculation is $O(nm)$, m is the number of convex hull vertices, so that sometimes its complexity is less than $O(n\log n)$, but since all n points of the initial set may belong to the convex hull and the Jarvis algorithm takes linear time to find each point, this leads to a total speedup of the algorithm of $O(n^2)$ in the worst case. Divide and Conquer algorithm divides the point set into two approximately equal, disjoint subsets and then recursively computes convex hulls of these sets and merges them, the speed of this algorithm depends heavily on the speed of merging the two convex hulls, and the merge takes $O(n)$ time. "Quickhull" algorithm is a class of algorithms created similar to quick order, which builds convex polygon by extreme points, the points inside the convex polygon must not be on the convex hull, and then the points outside the edges of the convex polygon are divided into subsets by the nearest number of edges, doing the same thing for each subset as for the initial set of points until there are no other points outside the built convex polygon, with a worst-

case complexity of $O(n^2)$ and an average of $O(n\log n)$. Andrew algorithm is a variant of the Graham scan algorithm, it uses lexicographic ordering of the coordinates of the points, that gives a huge advantage because floating point numbers and trigonometric instructions are not necessary. Andrew algorithm acts as a highly efficient ordering algorithm that theoretically reduces the time complexity of the convex hull algorithm to that of the ordering algorithm, with a lower bound on the time complexity of the ordering algorithm of $O(n\log n)$.

Point set convex hull algorithms can be divided into two classes based on whether they are ordered or not, ordering-based convex hull algorithms whose time complexity generally depends on the ordering algorithm, which has a lower bound of $O(n\log n)$, and another class that does not require ordering but whose time complexity is often higher than $O(n\log n)$. Though the minimum complexity of the convex hull algorithm is theoretically proven to be $O(n\log n)$ [1], its average performance is the same as the worst-case performance, so some works have been devoted to finding better algorithms [2,4,27,28]. More recently, we have also seen the use of convex hull as an auxiliary technique in CAD and CAM, Zhang et al. [32] aligned the damaged model with the nominal model by best-fitting their common convex hull centroids to assist in the additive manufacturing of damaged parts. Tsainis et al. [30] based on the convex hull algorithm to decentralize the tool surface into triangular faces to aid the calculation of the optimal tool orientation in 5-axis simultaneous CNC machining.

2.2 Bounding Box

Bounding box is a method for solving the optimal bounding space of a discrete point set in space, the main idea is to contain or approximate complex geometric objects with a slightly larger geometry (called a bounding box) with relatively simple properties [22]. A number of heuristics have been proposed to compute a bounding box containing a given point set [3].

Axis-aligned bounding box (AABB) is a cuboid with edges parallel to the spatial axes and the smallest volume, which has the advantage of being simple to build and little storage space, but is poorly compact and cannot be rotated accordingly when the object is rotated. Sphere bounding box (SBB) is defined as the smallest sphere containing an object, which is determined by the distance between the vertices furthest from the center of the sphere, and acts mainly on spherical objects. Oriented bounding box (OBB) is the smallest cuboid containing an object, it has an arbitrary orientation relative to the axes, and can be closer to the object than AABB and SBB. The key to the construction of the OBB is to find the optimal orientation by means of different methods. Representative of this is O'Rourke et al. [22], who used exact algorithm to solve OBB in polynomial time. Recently, principal component analysis (PCA) has become the main method for calculating OBB, the principal components of the point set are defined as the axes of the bounding box, however, when the model points are unevenly distributed, this may lead to unstable results from such methods. Dimitrov et al. [10] proposed a PCA boundary framework based on continuous sets on convex hull to overcome the phenomenon that the optimal solution may have unbounded difference. Chang et al. [7] proposed an approximate point set minimum volume bounding box algorithm, which is a combination of two optimization components, namely genetic algorithm and the Nelder-Mead algorithm, by combining the two methods, a good convergence speed can be obtained while avoiding local minima. At present, bounding box is mainly used in image processing, pattern recognition, collision detection and other fields.

3 MEASUREMENT SYSTEM AND PROPOSED METHOD

As shown in Figure 1, the geometric feature parameters of the metallic W-ring section profile include width b, height h_1, wave crest circle radius R_1, wave valley circle radius R_2, transition circle radius R_3, wave valley center distance b_1, wave height h_2 and wall thickness t. The profile

geometric feature is the basic feature that characterizes the overall size, and is the basis for constraining and calculating other geometric features, its parameters include width b and height h_1. The designed measurement system is based on optics, where the profile point cloud is obtained when the plane of light passes through the radial section of the metallic W ring, by processing the profile point cloud to obtain PGFPs.

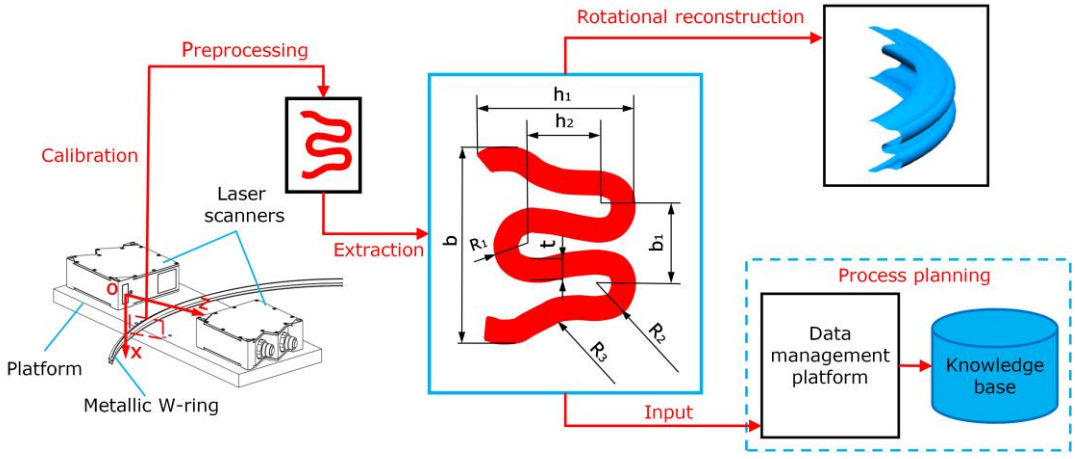

Figure 1: Schematic diagram for the inspection of PGFPs of metallic W-ring and their application.

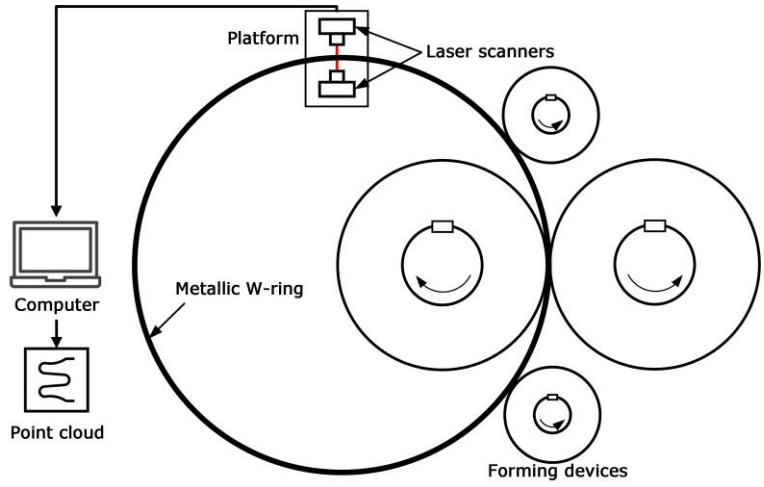

Figure 2: Measurement system for the geometric features of metallic ring.

The geometric feature measurement system of metallic ring is shown in Figure 2, consisting mainly of a computer, a platform and two laser scanners. Here, the calibration process of the measurement system is briefly introduced:

Step 1: The laser scanner is fixed on the platform, and the optical plane of the sensor is coplanar through the installation accuracy, and the effective measurement range of the two overlaps to the maximum extent, which constitutes the effective measurement range of the measurement system.

Step 2: The z-axis of one laser scanner is inverted to ensure that the internal and external profile point clouds of the object are unified in the coordinate system, at which point the internal and external profile point clouds are placed squarely in the coordinate system based on the geometric accuracy of the measurement system.

Step 3: In order to further reduce the influence of the geometric error of the measurement system, the corresponding calibration objects and algorithms (mainly for line fitting and circle fitting algorithms) are designed, the calibration objects consist mainly of a cuboid and a cylinder. The angles of the two sets of opposite edges in the inner and outer profiles of the cuboid are used to calculate the amount of rotation in the z-x plane, and the circular coordinates of the inner and outer circular profiles of the cylinder are used to calculate the amount of translation in the z and x directions.

Step 4: Based on the calculated rotation and translation, the inner profile point cloud is transformed to obtain the profile measurement point cloud.

After calibration and pre-processing of the measurement data (such as stitching, denoising, etc.), a point cloud of the inner and outer profiles of the metallic ring section can be obtained. The designed measurement system has the following advantages:

(1) It can be easily installed and integrated into the metallic ring forming device for on-machine, non-contact, non-destructive measurement.

(2) Benefitting from the designed calibration objects and algorithms, the obtained point cloud of the metallic ring section profile is placed squarely in the measuring coordinate system, that is, the line connecting the center of the wave valley circles is at a small angle to the x-axis of the measurement coordinate system, satisfying the accuracy of the feature parameters extraction.

Bounding box is widely used in collision and intersection detection, it can effectively characterize the PGFPs of objects in a specific scene, but there are certain limitations in extracting PGFPs from metallic W-ring. In this article, we propose an adaptive bounding box based multi-pass PGFPs extraction method based on the following considerations. Firstly, through an optical-based on-machine measurement platform, a 2D point cloud of the section profile of the metallic W-ring is obtained. The bounding rectangle is a dimensionality reduction representation of the bounding box from 3D space to 2D space, it is an effective measure of the space enclosed by discrete point sets. Therefore, the bounding rectangle is used to characterize the bounding box of the 2D point cloud of the section profile of the metallic W-ring. Secondly, the metallic W-ring has a large difference in shape and a large number of points in the section profile point cloud during the multi-pass rolling forming process, which makes the direct building of bounding rectangle complex, unstable and inefficient. Therefore, by calculating the convex hull of the section profile point cloud, the different profile point cloud is transformed into the corresponding convex hull with similar shape and relatively few points to improve the stability and efficiency of building the bounding rectangle. Thirdly, we find that the PGFPs of each pass of the metallic ring can be effectively characterized by means of a minimum area bounding rectangle (MABR), the method for building the bounding box based on principal component analysis (PCA-OBB) is popular, but the measurement section profile of the metallic W-ring may not conform to the theoretical shape, such as the different lengths of the sealing lips on both sides, this can lead to an uneven distribution of points and make errors in determining the orientation. Benefiting from the calibration of the optical measuring system, we determine whether there is a significant difference in length between the sealing lips of the two sides of the metallic W-ring based on the slope of the vertices of the convex hull, an adaptive bounding box that more closely approximate the section profile point cloud is built. The adaptive bounding box is composed of OBB and AABB, for the point cloud of the metallic W-ring with theoretical shape, the PGFPs are extracted by OBB, the orientation of OBB selects the vertical orientation of the edge of the convex hull corresponding to the bounding rectangle, in order to more closely enclose the point clouds, and for the point clouds of the section profile of the metallic W-ring with varying seal lip lengths, we define the height based on the longer side of the sealing lip and extract their PGFPs by means of AABB. The method makes full use of the calibration of the

optical measurement system and the section profile information during the rolling forming process of the metallic W-ring to improve accuracy, robustness and efficiency.

In summary, the adaptive bounding box based multi-pass PGFPs extraction method is shown in Figure 3.

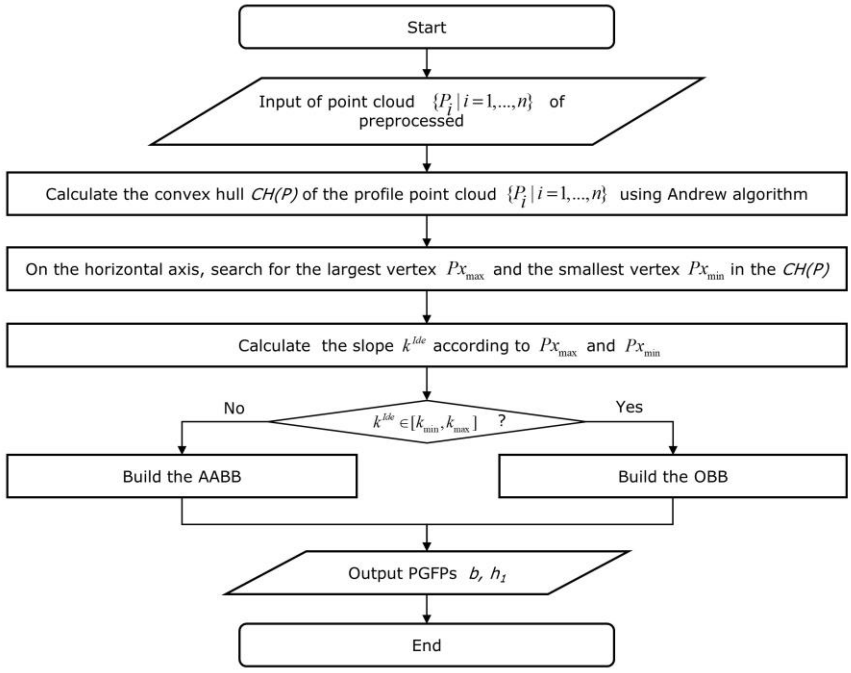

Figure 3: Adaptive bounding box based multi-pass PGFPs extraction method.

4 ADAPTIVE BOUNDING BOX BASED MULTI-PASS PGFPS EXTRACTION METHOD

In this section, the method for calculating convex hull, convex hull vertices slope-based profile recognition method, and the building of AABB and OBB are given.

4.1 Calculate Convex Hull

Define the 2D Euclidean space as E^2, for a given point set $\{P_i|i=1,...,n\}$ on the plane, the plane region

$$D = \{d \in E^2 \mid d = \sum_{i=1}^{n} t_i P_i, t_i \geq 0, \sum_{i=1}^{n} t_i = 1\} \tag{4.1}$$

is the convex set generated by $\{P_i|i=1,...,n\}$. The smallest convex set containing $\{P_i|i=1,...,n\}$ is defined as the convex hull, denoted as $CH(P)$. A review of classical convex hull algorithms is given in [6] and shows that the "Quickhull" algorithm and the Andrew algorithm have the best performance compared to other algorithms, the " Quickhull" algorithm has a better performance in the initial set of points with uniform or gaussian distribution, the Andrew algorithm has an advantage in the uneven distribution. Considering that the measurement data may be unevenly

distributed after preprocessing, we choose the Andrew algorithm. Andrew algorithm is a variant of the Graham scan algorithm, to illustrate the differences and advantages of Andrew algorithm and Graham scan algorithm, we first introduce the Graham scan algorithm. The steps of Graham Scan algorithm are as follows:

Step 1: The polar coordinate system is built by selecting the lower left point in the given point set $\{P_i|i=1,\ldots,n\}$ as the origin, give priority to the lowermost, and record the origin as P_0.

Step 2: Order the point set. The polar angles of the remaining points in the polar coordinate system are calculated, and the points are ordered in ascending order of polar angle. If there are multiple points with the same polar angle, only the distal point is retained. The set of points after ordering is denoted $\{P_1,P_2,\ldots,P_m\}$.

Step 3: Scan the set of ordered points and find the vertices of the convex hull. Initialize a stack S to hold the convex hull vertices and let P_0 and P_1 in the stack. Let $S(0)=P_0$, $S(1)=P_1$, and note that the top element of the stack is $S(k)$. If the path formed by the points $S(k\text{-}1)$, $S(k)$ and P_i is a left turn, then P_i is in the stack, $k=k+1$, and $S(k)=P_i$, as shown in Figure 4(a). If the path formed by the points $S(k\text{-}1)$, $S(k)$ and P_i is a right turn, then $S(k)$ is out of the stack and $k=k-1$, $S(k)=P_i$, otherwise, the path formed by the three points $S(k\text{-}1)$, $S(k)$ and P_i needs to be re-judged to turn, as shown in Figure 4(b). And so on, until all points are traversed, the scan result is shown in Figure 4(c).

Step 4: Output in order all the points saved in the stack, which are the vertices of the convex hull, denoted as $CH(P)$.

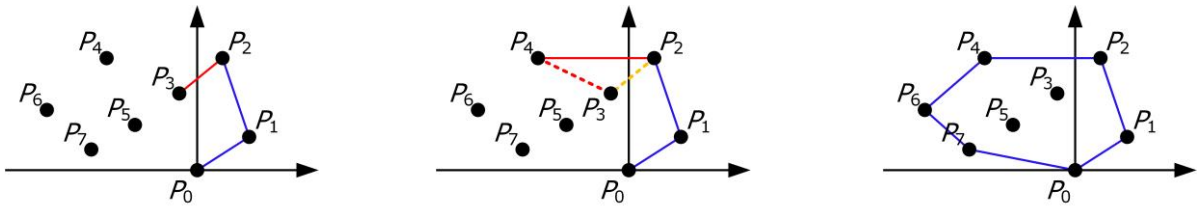

(a) (b) (c)

Figure 4: Calculate convex hull based on the Graham Scan algorithm: (a) P_1, P_2, P_3 left, P_3 in the stack, (b) P_2, P_3, P_4 turn right, P_3 out of stack, P_1, P_2, P_4 left turn, P_4 in the stack, and (c) Complete convex hull.

The Graham Scan algorithm needs to calculate the polar angle and order according to the size of the polar angle, while the Andrew algorithm only orders by the coordinate size during the ordering process, avoiding unnecessary floating-point numbers and trigonometric instructions. Therefore, compared with the original Graham algorithm, Andrew algorithm is faster and has better numerical stability. The steps of Andrew algorithm are as follows:

Step 1: Order all the points in the point set from smallest to largest in terms of horizontal coordinates, and for points with the same horizontal coordinates, order them from smallest to largest in terms of vertical coordinates. The ordering result is $\{P_1,P_2,\ldots,P_n\}$, at this point P_1 and P_n must be the vertices of the convex hull.

Step 2: Start from P_1 and search to the right to find the lower half of the convex hull, as shown in Figure 5(a). The algorithm for determining the convex hull vertices in this step is the same as step 3 of the Graham scan algorithm.

Step 3: Start from P_n and search to the left to find the upper half of the convex hull, as shown in Figure 5(b).

Step 4: Combine the results of step 2 with step 3 to obtain the complete convex hull $CH(P)$.

Figure 5: Compute convex hull based on the Andrew algorithm: (a) The lower half of the convex hull, (b) The upper half of the convex hull.

The convex hull of the section profile point cloud of the fourth forming pass of the metallic W-ring is built using the Andrew algorithm, as shown in Figure 6.

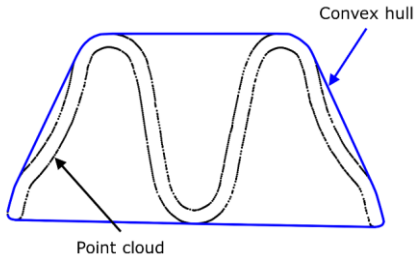

Figure 6: Convex hull of the point cloud of the fourth forming pass of the metallic W-ring.

4.2 Profile Identification Method

Metallic W-rings can be divided into two categories according to their section shape, one category is in accordance with the theoretical model, with an overall symmetrical structure and the sealing lips on both sides do not have obvious length differences, another category has a forming defect, mainly manifested in significantly different lengths of the sealing lips, as shown in Figure 7, for this forming defect, the slope of the vertices in the horizontal orientation of the convex hull is used to identify it. The steps of convex hull vertices slope-based profile identification method are as follows:

Step 1: Extract the vertices of the convex hull, the largest vertex and the smallest vertex in the horizontal orientation, when is the same, take the smallest point in the vertical orientation, denoted as

$$Px_{\max} = (x_{P_{X\max}}, z_{P_{X\max}}) \tag{4.2}$$

$$Px_{\min} = (x_{P_{X\min}}, z_{P_{X\min}}) \tag{4.3}$$

Step 2: Calculate the slope of point $Px_{\max}$ and point $Px_{\min}$

$$k^{Ide} = \frac{z_{P_{X\max}} - z_{P_{X\min}}}{x_{P_{X\max}} - x_{P_{X\min}}} \tag{4.4}$$

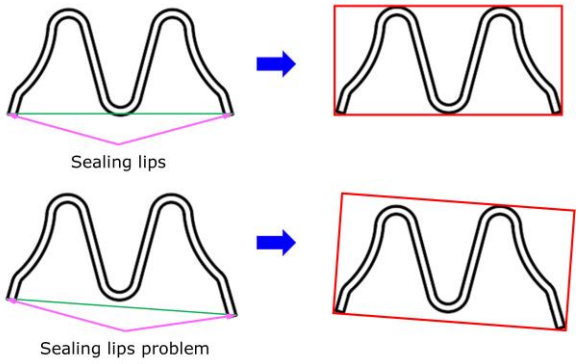

Figure 7: Inaccurate bounding box due to sealing lips problem.

Step 3: Determine whether k^{Ide} belongs to the theoretical sealing lip slope interval $[k_{\min}, k_{\max}]$, when $k^{Ide} \in [k_{\min}, k_{\max}]$, build OBB according to $CH(P)$, and when $k^{Ide} \notin [k_{\min}, k_{\max}]$, build AABB according to $CH(P)$.

4.3 Building of OBB

The OBB in 2D space is built on the basis of rotating calipers [29], an algorithm that can be solved in linear time, the principle is to use a pair of parallel lines to clamp a convex polygon and compute all the bounding rectangles by rotating the parallel lines, from which the OBB, i.e. MABR, is determined. Freeman et al. [12] proved that at least one edge of the MABR of a convex polygon coincides with an edge in that convex polygon, which simplifies the computation to a great extent. The steps for solving the convex hull minimum bounding rectangle using the rotating calipers are as follows:

Step 1: Extract the maximum and minimum vertices of the convex hull vertices in the orientation of the horizontal and vertical coordinates, denoted as $Px_{\max}$, $Px_{\min}$, $Pz_{\max}$ and $Pz_{\min}$.

Step 2: Through the four vertices, two sets of parallel lines are identified to build the bounding rectangle of the convex hull, as shown in Figure 8(a).

Step 3: Determine whether there is an edge in the bounding rectangle that coincides with an edge in the convex polygon. If so, calculate the area of the rectangle, save it as the rectangle area minimum, and record the coordinates of the four vertices of the rectangle. Otherwise, set the minimum value of the area of the rectangle to infinity.

Step 4: Reconstruct the external rectangle by rotating the two sets of parallel lines clockwise until one of the lines coincides with an edge in the convex polygon, as shown in Figure 8(b). Calculate the area of the rectangle, compare it with the current minimum value of the rectangle area, and if it is less than the current minimum, update the area of the rectangle with the coordinates of the rectangle vertices.

Step 5: Repeat step 4 until the overall rotation angle exceeds 90°.

Step 6: Output the coordinates of the vertices of the bounding rectangle.

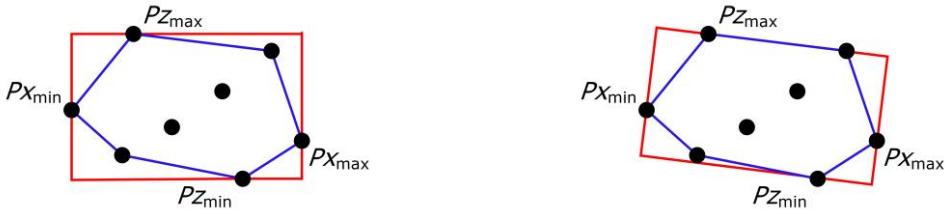

(a) (b)

Figure 8: Build the MABR of the convex hull based on the rotating calipers: (a) Build the bounding rectangle, (b)Update the bounding rectangle.

At least one edge of the bounding rectangle coincides with one edge of the convex polygon, and the vertical orientation of the coincident edge is selected as the orientation of the OBB. The OBB corresponding to the point cloud of the section profile of the fourth forming pass of the metallic W-ring is built based on the rotating calipers, as shown in Figure 9, the width and height of the OBB are used to represent the section profile width b and height h_1 of the metallic W-ring.

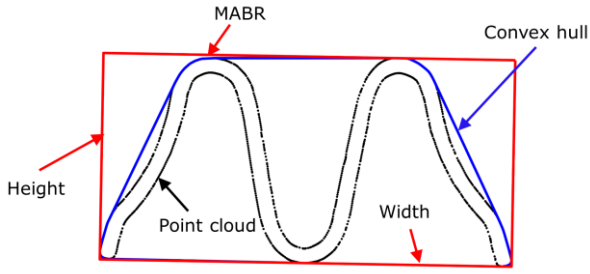

Figure 9: MABR of metallic W-ring section profile point cloud.

4.4 Building of AABB

AABB is a hexahedron containing objects and with all edges parallel to the coordinate axes, represented in 2D space as an bounding rectangle parallel to the coordinate axes, and solving for AABB proceeds as follows:

Step 1: Extract the maximum and minimum vertices of the convex hull vertices in the orientation of the horizontal and vertical coordinates, denoted as $Px_{\max}$, $Px_{\min}$, $Pz_{\max}$ and $Pz_{\min}$.

Step 2: Build the bounding rectangle of the convex hull by identifying two sets of edges parallel to the horizontal and vertical axes through the four vertices, as shown in Figure 8 (a).

Step 3: Output the coordinates of the vertices of the bounding rectangle.

Similar to figure 9, the width and height of the AABB are used to represent the section profile width b and height h_1 of the metallic W-ring.

5 A METHOD TO INSPECT PGFPS FROM CTWRPIC AND EXPERIMENTAL SETUP

Based on the adaptive bounding box based multi-pass PGFPs extraction method, and use the designed optical measurement system, a method to inspect PGFPs from CTWRPIC is established, as shown in Figure 10.

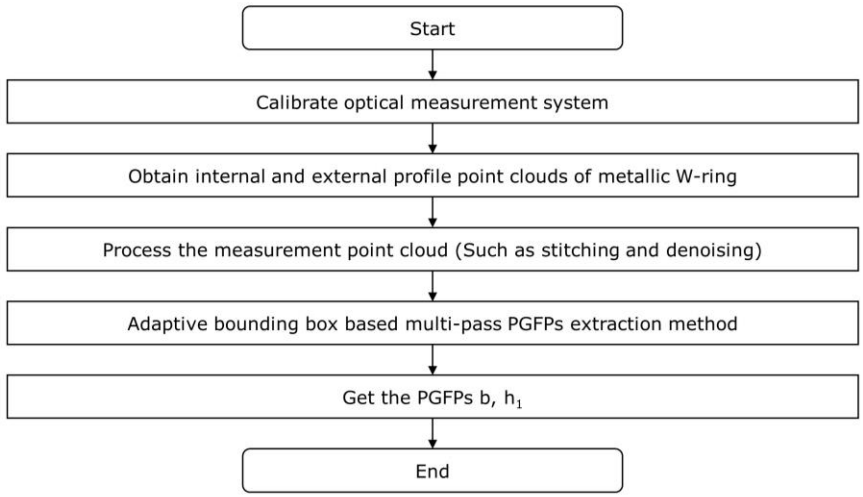

Figure 10: A method to inspect PGFPs from CTWRPIC.

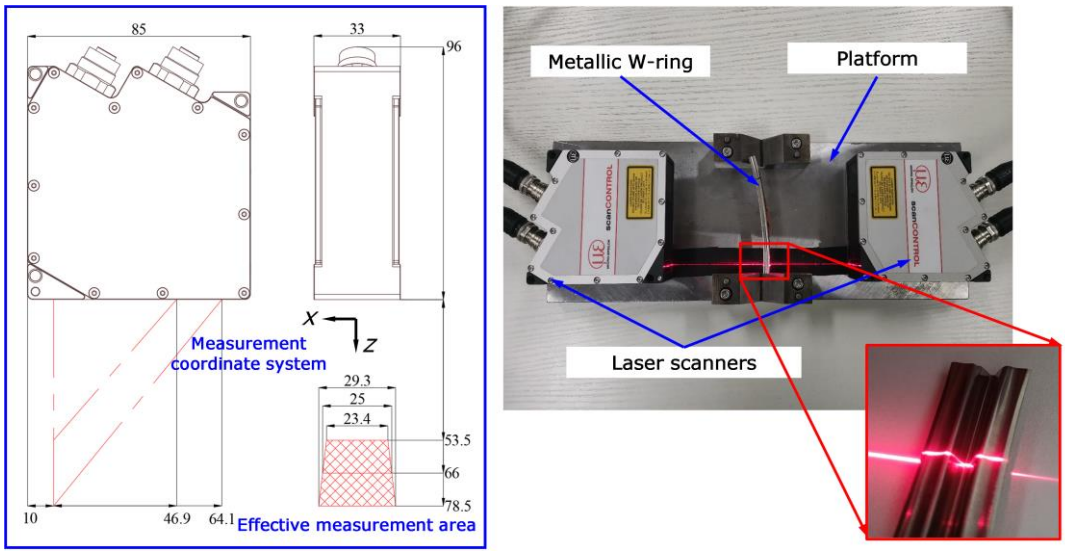

Figure 11: The measurement system.

The experimental setup is as follows. First, the optical measurement system is equipped with two-line laser scanners of the same model, the line laser scanner has a z-axis reference resolution of 2 μm and an x-axis resolution of 1280 points/profile, and other parameters are shown in the figure 11. Second, in order to verify the robustness of our proposed method, we choose metallic W-ring samples from six rolling forming passes as the measurement object, as shown in Figure 12. Third, destructive inspection is used in the experiments and the measurements are used as a reference model. Fourth, to verify the accuracy of the proposed method, comparative experiments are conducted using several classical and representative methods, including Rotary calipers-based OBB (RC-OBB), AABB and PCA-OBB. The relative error of their extraction results from those of traditional destructive inspection are used as the evaluation criterion. In this article, the above methods are implemented in Visual Studio 2017.

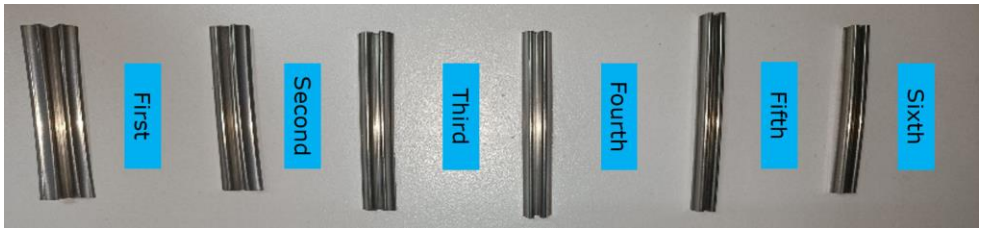

Figure 12: Metallic W-ring samples from six rolling forming passes.

6 RESULTS AND DISCUSSION

Figure 13 shows the traditional destructive section measurement data and the preprocessing data of our designed measurement platform. We can observe that the metallic W-ring appears obvious forming defects after the fifth pass. i.e. different lengths of the sealing lips. In order to verify the feasibility of our proposed method, we use the bounding box based multi-pass PGFPs extraction method to extract the PGFPs, and compared with the above methods. The feature parameter extraction results are shown in Figure 14.

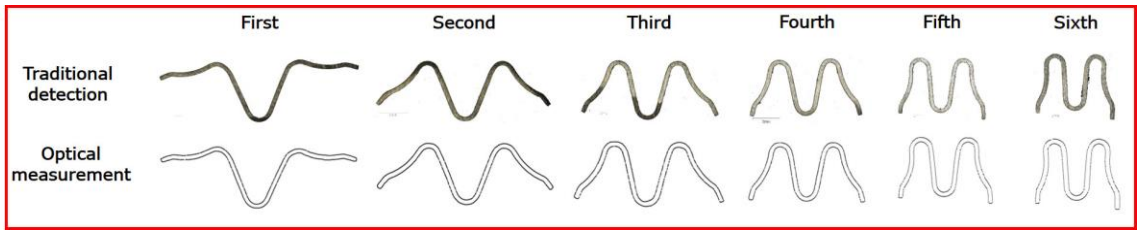

Figure 13: Traditional destructive measurement data and our designed optical measurement data.

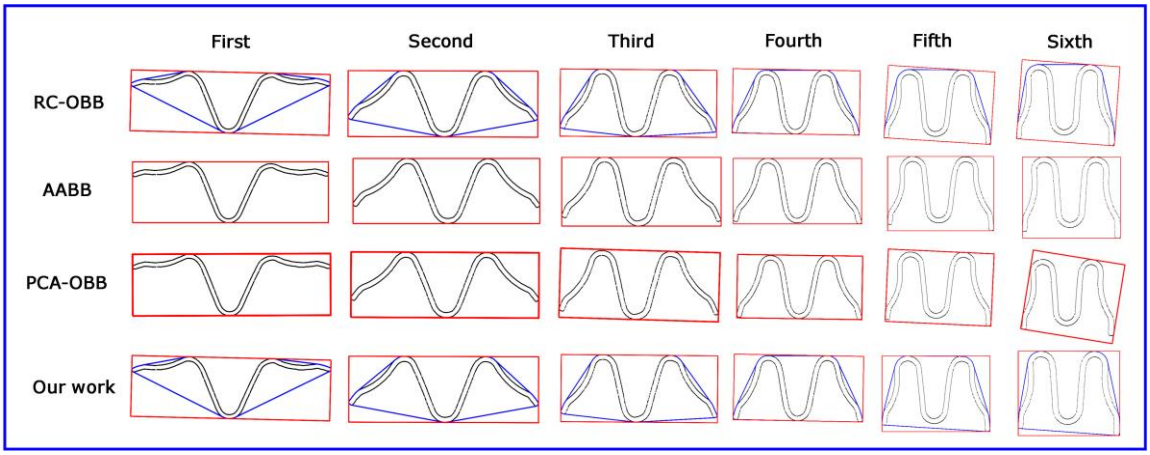

Figure 14: PGFPs of metallic W-ring in six forming passes under four methods.

As shown in Figure 14, the black is the metallic W-ring section profile point cloud, the blue polygon indicates the convex hull and the red rectangle indicates the bounding box. As can be seen from

Tables 1 and 2, our method is more accurate in extracting the PGFPs of the metallic W-ring with a relative error of only 0.01.

To further compare our work with other methods we have perform a qualitative analysis. RC-OBB calculates the MABR based on the convex hull, in the first four passes, there is no significant difference in length between the sealing lips on either side of the metallic W-ring, and the shape is in accordance with the theoretical model. In the fifth and sixth passes, the calculated convex hull has an obvious asymmetric structure in the z-axis orientation, and the MABR of the convex hull is always built based on the non-parallel bottom edge of the convex hull, which does not more closely approximate the profile point cloud of the metallic W-ring, and leads to significant errors in the extracted height parameters, as shown in Table 2. PCA-OBB estimates the orientation of the OBB by calculating the feature vector, which is unstable when the profile point cloud is unevenly distributed, therefore, in the fifth and sixth passes, the difference in length between the sealing lips on both sides of the metallic W-ring resulted in an uneven distribution of the point cloud, and the calculated bounding box at this point did not effectively characterize the profile geometry. Benefiting from the optical measuring system and calibration, the obtained point cloud of the metallic W-ring section is placed squarely in the measuring coordinate system, therefore, AABB can effectively characterize the PGFPs of the section point cloud for six passes and the relative error of the extracted geometric features is low. However, it is not realistic to place them exactly in the measurement coordinate system and small angular deviations are inevitable, so the robustness of AABB can be further optimized. Second, AABB's PGFPs extraction is similar in principle to traditional destructive inspection in that it calculates feature parameters based on coordinate vertices. The advantage of our method lies in the establishment of adaptive bounding box, which identifies the profile shape for the existence of forming defects based on the slope of the convex hull vertices. For the point cloud of the section profile of the metallic W-ring that conforms to the theoretical shape, that is, the first four passes in this experiment, we extract their PGFPs through OBB. For the metallic W-ring with different lengths of sealing lips, we define the height according to the longer side of the sealing lip, and jointly calibrate and AABB extract its PGFPs, which overcomes the shortcomings of single OBB and AABB. As shown in Table 2, in terms of width b, the average relative error of our method is not the lowest, but compared with the minimum value obtained by PCA-OBB, the difference is only 0.002. In terms of height h_1, the average relative error of the method in this paper is the lowest, and the difference between PCA-OBB and the method in this article is 0.010, therefore, our method is more accurate in height h_1 extraction. At the same time, in terms of the overall average relative error of width and height, our method in still achieves the minimum value.

Forming pass		*Standard*	*RC-OBB*	*PCA-OBB*	*AABB*	*This work*
Width (mm)	First	13.915	13.891	13.895	13.895	13.891
	Second	11.939	11.871	11.871	11.871	11.871
	Third	9.697	9.682	9.685	9.680	9.682
	Fourth	8.222	8.268	8.268	8.266	8.268
	Fifth	6.552	6.557	6.557	6.551	6.551
	Sixth	5.780	5.720	5.759	5.702	5.702
Height (mm)	First	4.218	4.244	4.320	4.309	4.244
	Second	4.099	4.120	4.123	4.128	4.120
	Third	4.132	4.148	4.192	4.163	4.148
	Fourth	4.274	4.180	4.190	4.219	4.180
	Fifth	4.726	4.465	4.466	4.597	4.597
	Sixth	4.836	4.624	4.947	4.730	4.730

Table 1: Results of PGFPs extraction under five methods.

Forming pass		*RC-OBB*	*PCA-OBB*	*AABB*	*This work*
Width	First	0.002	0.001	0.001	0.002
	Second	0.006	0.006	0.006	0.006
	Third	0.002	0.001	0.002	0.002
	Fourth	0.006	0.006	0.005	0.006
	Fifth	0.001	0.001	0.000	0.000
	Sixth	0.010	0.004	0.013	0.013
	Average	**0.005**	**0.003**	**0.005**	**0.005**
Height	First	0.006	0.024	0.022	0.006
	Second	0.005	0.006	0.007	0.005
	Third	0.004	0.015	0.008	0.004
	Fourth	0.022	0.020	0.013	0.022
	Fifth	0.055	0.055	0.027	0.027
	Sixth	0.044	0.023	0.022	0.022
	Average	**0.023**	**0.024**	**0.017**	**0.014**
	Average	**0.014**	**0.014**	**0.011**	**0.010**

Table 2: Relative error of PGFPs under four extraction methods.

7 CONCLUSION

In this article, an adaptive bounding box based multi-pass PGFPs extraction method is proposed, for extracting the PGFPs of the section profile of metallic W-ring under multiple rolling forming passes, which consists mainly of convex hull calculation, forming defect identification, and building of adaptive bounding box. Specifically, converts the section profile point cloud of each pass with large shape difference into the corresponding convex hull with similar shape, so as to improve the efficiency and stability of bounding box. Second, the slope of the convex hull vertices is used to identify whether the metallic W-ring has forming defects, so as to build an adaptive bounding box that more closely approximate the section profile point cloud. Therefore, our method is suitable for extracting PGFPs from CTWRPIC.

In addition, based on the proposed method and the optical measurement system, we further propose a method to inspect PGFPs from CTWRPIC. In order to evaluate the performance of our method, the PGFPs extracted by the adaptive bounding box based multi-pass PGFPs extraction method and other methods are compared with the results of traditional destructive inspection, and the results show that compared with other PGFPs extraction methods, the proposed method has better accuracy and robustness and is of practical value in engineering applications.

ACKNOWLEDGEMENT

The work described in this article was supported by a grant from the National Science and Technology Major Project of China (Project no. J2019-VII-0014-0154).

Haonan Pei, http://orcid.org/0000-0002-1350-1299
Ming Luo, http://orcid.org/0000-0003-1648-3425
Sizhe Du, http://orcid.org/0000-0003-2455-3358

REFERENCES

[1] Andrew, A.M.: Another efficient algorithm for convex hulls in two dimensions, Information Pr ocessing Letters, 9(5), 1979, 216-219. https://doi.org/10.1016/0020-0190(79)90072-3.

[2] Barber, C. B.; Dobkin, D. P.; Huhdanpaa, H.: The Quickhull Algorithm for Convex Hulls, ACM Transactions on Mathematical Software, 22 (4), 1996, 469–483. https://doi.org/10.1145/235815.235821.
[3] Barequet, G.; Har-Peled, S.: Efficiently Approximating the Minimum-Volume Bounding Box of a Point Set in Three Dimensions, Journal of Algorithms, 38 (1), 2001, 91–109. https://doi.org/10.1006/jagm.2000.1127.
[4] Beltran, A.; Mendoza, S.: SymmetricHull: A Convex Hull Algorithm Based on 2D Geometry and Symmetry, IEEE Latin America Transactions, 16 (8),2018, 2289–2295. https://doi.org/10.1109/TLA.2018.8528248.
[5] Bykat, A.: Convex Hull of a Finite Set of Points in Two Dimensions. Information Processing Letters,7 (6), 1978, 296–298. https://doi.org/10.1016/0020-0190(78)90021-2.
[6] Chadnov, R. V.; Skvortsov, A. V.: Convex Hull Algorithms Review, The 8th Russian-Korean International Symposium on Science and Technology, 2, 2004, 112–115. https://doi.org/10.1109/KORUS.2004.1555560.
[7] Chang, C.-T.; Gorissen, B.; Melchior, S.: Fast Oriented Bounding Box Optimization on the Rotation Group SO (3,R), ACM Transactions on Graphics, 30 (5), 2011, 1–16. https://doi.org/10.1145/2019627.2019641.
[8] Chen, X.; Wang, Y.: Analysis of Fatigue Life in High Temperature of W Pattern Sealing Rings Used in Aircraft Engine, Applied Mechanics and Materials, 496–500, 2014, 571–574. https://doi.org/10.4028/www.scientific.net/AMM.496-500.571.
[9] Cheng, Y.; Li, W.; Jiang, C.; Wang, G.; Xu, W.; Peng, Q.: A Novel Cooling Hole Inspection Method for Turbine Blade Using 3D Reconstruction of Stereo Vision, Measurement Science and Technology, 33 (1), 2022, 015018. https://doi.org/10.1088/1361-6501/ac39d0.
[10] Dimitrov, D.; Knauer, C.; Kriegel, K.; Rote, G.: Bounds on the Quality of the PCA Bounding Boxes, Computational Geometry, 42 (8) 2009, 772–789. https://doi.org/10.1016/j.comgeo.2008.02.007.
[11] Eddy, W. F.: A New Convex Hull Algorithm for Planar Sets, ACM Transactions on Mathematical Software, 3 (4), 1977, 398–403. https://doi.org/10.1145/355759.355766.
[12] Freeman, H.; Shapira, R.: Determining the minimum-area encasing rectangle for an arbitrary closed curve, Communications of the ACM, 18(7),1975, 409-413. https://doi.org/10.1145/360881.360919.
[13] Gadelmawla, E. S.: Computer Vision Algorithms for Measurement and Inspection of Spur Gears, Measurement, 44 (9), 2011, 1669–1678. https://doi.org/10.1016/j.measurement.2011.06.023.
[14] Graham, R.L.: An efficient algorithm for determining the convex hull of a finite planar set, Information Processing Letters, 1(4), 1972,73-82. https://doi.org/10.1016/0020-0190(72)90045-2.
[15] Graham, R. L.; Frances Yao, F.: Finding the Convex Hull of a Simple Polygon. Journal of Algorithms, 4 (4), 1983, 324–331. https://doi.org/10.1016/0196-6774(83)90013-5.
[16] Jarvis, R. A.: On the Identification of the Convex Hull of a Finite Set of Points in the Plane, Information Processing Letters, 2 (1), 1973, 18–21. https://doi.org/10.1016/0020-0190(73)90020-3.
[17] Ke, Y.; Fan, S.; Zhu, W.; Li, A.; Liu, F.; Shi, X.: Feature-based reverse modeling strategies. Computer-Aided Design, 38(5),2006, 485-506. https://doi.org/10.1016/j.cad.2005.12.002.
[18] Li, W.; Wu, A.; Li, Z.; Zhang, G.; Yu, W.: A New Calibration Method between an Optical Sensor and a Rotating Platform in Turbine Blade Inspection, Measurement Science and Technology. 28 (3),2017, 035009. https://doi.org/10.1088/1361-6501/aa50df.
[19] Li, W.; Zhou, L.; Yan, S.: A Case Study of Blade Inspection Based on Optical Scanning Method, International Journal of Production Research, 53 (7), 2015, 2165–2178. https://doi.org/10.1080/00207543.2014.974851.
[20] Liu, Z. G.; Li, Y. F.; Bao, P.: A Method for Efficient Measurement and Reconstruction of Free Form Surfaces Using Vision Guidance, Computer-Aided Design and Applications, 1 (1–4), 2004, 83–90. https://doi.org/10.1080/16864360.2004.10738246.

[21] Martínez-Pellitero, S.; Barreiro, J.; Cuesta, E.; Fernández-Abia, A. I.: Knowledge Base Model for Automatic Probe Orientation and Configuration Planning with CMMs, Robotics and Computer-Integrated Manufacturing, 49, 2018, 285–300. https://doi.org/10.1016/j.rcim.2017.08.012.
[22] O'Rourke, J.: Finding Minimal Enclosing Boxes. International Journal of Computer and Information Sciences, 14 (3), 1985, 183–199. https://doi.org/10.1007/BF00991005.
[23] Peng, G.; Zhang, Z.; Li, W.: Computer Vision Algorithm for Measurement and Inspection of O-Rings, Measurement, 94, 2016, 828–836. https://doi.org/10.1016/j.measurement.2016.09.012.
[24] Preparata, F. P.; Hong, S. J.: Convex Hulls of Finite Sets of Points in Two and Three Dimensions, Communications of the ACM, 20 (2), 1977, 87–93. https://doi.org/10.1145/359423.359430.
[25] Sang, Y.; Yan, Y.; Yao, C.; He, G.: A New Scanning Lines Distribution Strategy for the Form Error Evaluation of Freeform Surface on CMM, Measurement, 181, 2021, 109578. https://doi.org/10.1016/j.measurement.2021.109578.
[26] Singh S K.; Mohanty A M.: A Survey of Automated Process Planning Approaches in Machining, International Journal of Engineering and Management Research, 8(6), 2018, 81-88. https://doi.org/10.31033/ijemr.8.6.02.
[27] Stein, A.; Geva, E.; El-Sana, J.: CudaHull: Fast Parallel 3D Convex Hull on the GPU. Computers & Graphics, 36 (4) 2012, 265–271. https://doi.org/10.1016/j.cag.2012.02.012.
[28] Tang, M.; Zhao, J.; Tong, R.; Manocha, D.: GPU Accelerated Convex Hull Computation. Computers & Graphics ,36 (5), 2012, 498–506. https://doi.org/10.1016/j.cag.2012.03.015.
[29] Toussaint, G.T.: Solving geometric problems with the rotating calipers. Proc. IEEE MELECON' 83, Athens, Greece, 1983: 1-8.
[30] Tsainis, A. M.; Papazafeiropoulos, G.; Stergiou, C.: A Novel Convex Hull Method for Optimum Multi-Point 5-Axis Tool Positioning for Machining of Complex Sculptured Surfaces, The International Journal of Advanced Manufacturing Technology, 103 (9–12), 2019, 4369–4383. https://doi.org/10.1007/s00170-019-03833-9.
[31] Wang, Z.; Yin, M.; Ou, D.; Xie, L.; Liu, H.; Yin, G.: Optical Measurement Method for Blade Profiles Based on Blade Self-Features, IEEE Transactions on Industrial Electronics. 69 (2), 2022, 2067–2076. https://doi.org/10.1109/TIE.2021.3062213.
[32] Zhang, X.; Cui, W.; Liou, F.: Voxel-Based Geometry Reconstruction for Repairing and Remanufacturing of Metallic Components Via Additive Manufacturing, International Journal of Precision Engineering and Manufacturing-Green Technology, 8 (6), 2021, 1663–1686. https://doi.org/10.1007/s40684-020-00291-7.
[33] Zhang, Y.; Zhou, Z.; Tang, K.: Sweep Scan Path Planning for Five-Axis Inspection of Free-Form Surfaces, Robotics and Computer-Integrated Manufacturing, 49, 2018, 335–348. https://doi.org/10.1016/j.rcim.2017.08.010.